Abstract

Anti-aging and pro-longevity effects of caloric restriction
——Remodeling of white adipose tissue and activation of lipid metabolism——

Yuka Sudo, Naoyuki Okita and Yoshikazu Higami

Molecular Pathology and Metabolic Disease, Faculty of Pharmaceutical Sciences, Tokyo University of Science, Chiba 278-8510, Japan

Caloric restriction (CR) can extend both mean and maximum lifespans, and delay the onset of several age-related patho-physiological changes. It has been suggested that the beneficial actions of CR may be involved in several adaptive responses against food shortage including suppression of growth hormone (GH) /insulin like growth factor 1 (IGF-1) signaling, reduced oxidative stress, activation of surtuin and enhanced mitochondrial biogenesis. However, the exact underlying mechanisms are still debatable. Recently, we found that CR promotes metabolic remodeling with the activation of *de novo* fatty acid biosynthesis, mitochondrial biogenesis and reduced oxidative stress in the adipose tissue via sterol regulatory element binding protein (SREBP) 1c, a master transcriptional factor of fatty acid biosynthesis. Our findings suggest that SREBP1c might play an important role in the anti-aging and pro-longevity actions of CR in the GH/IGF-1-independent manner.

(The Autonomic Nervous System, 50: 192 ～ 195, 2013)

Biochemical and Biophysical Research Communications 446 (2014) 91–97

Contents lists available at ScienceDirect

Biochemical and Biophysical Research Communications

journal homepage: www.elsevier.com/locate/ybbrc

Inhibitory effect of p53 on mitochondrial content and function during adipogenesis

Naoyuki Okita [a,b,1,*], Natsumi Ishikawa [a,1], Yuhei Mizunoe [a], Misako Oku [a], Wataru Nagai [a], Yuki Suzuki [a], Shingo Matsushima [a], Kentaro Mikami [a], Hitoshi Okado [a], Takashi Sasaki [b,c], Yoshikazu Higami [a,*]

[a] Laboratory of Molecular Pathology and Metabolic Disease, Faculty of Pharmaceutical Sciences, Tokyo University of Science, 2641 Yamazaki, Noda-shi, Chiba 278-0022, Japan
[b] Department of Internal Medicine Research, Sasaki Institute, Sasaki Foundation, 2-2 Kandasurugadai, Chiyoda-ku, Tokyo 101-0062, Japan
[c] Division of Translational and Molecular Medicine, Research Center for Medical Sciences, The Jikei University School of Medicine, 163-1 Kashiwashita, Kashiwa-shi, Chiba 277-8567, Japan

ARTICLE INFO

Article history:
Received 8 February 2014
Available online 21 February 2014

Keywords:
p53
Ppargc1a
Adipogenesis
Mitochondrial biogenesis

ABSTRACT

The p53 protein is known as a guardian of the genome and is involved in energy metabolism. Since the metabolic system is uniquely regulated in each tissue, we have anticipated that p53 also would play differential roles in each tissue. In this study, we focused on the functions of p53 in white adipose tissue (adipocytes) and skeletal muscle (myotubes), which are important peripheral tissues involved in energy metabolism. We found that in 3T3-L1 preadipocytes, but not in C2C12 myoblasts, p53 stabilization or overexpression downregulates the expression of *Ppargc1a*, a master regulator of mitochondrial biogenesis. Next, by using p53-knockdown C2C12 myotubes or 3T3-L1 preadipocytes, we further examined the relationship between p53 and mitochondrial regulation. In C2C12 myoblasts, p53 knockdown did not significantly affect *Ppargc1a* expression and mtDNA, but did suppress differentiation to myotubes, as previously reported. However, in 3T3-L1 preadipocytes and mouse embryonic fibroblasts, p53 downregulation enhanced both differentiation into adipocytes and mitochondrial DNA content. Furthermore, p53-depleted 3T3-L1 cells showed increase in mitochondrial proteins and enhancement of both Citrate Synthase and Complex IV activities during adipogenesis. These results show that p53 differentially regulates cell differentiation and mitochondrial biogenesis between adipocytes and myotubes, and provide evidence that p53 is an inhibitory factor of mitochondrial regulation in adipocyte lineage.

1. Introduction

Tumor suppressor p53, which is known as a genome guardian that functions in various intrinsic and extrinsic stresses, is one such protein [1]. Under stress conditions, p53 is stabilized and activated via post-translational modifications such as phosphorylation and acetylation, whereas under non-stress conditions, p53 protein is maintained at low levels by proteasomal degradation via ubiquitination involving ubiquitin E3 ligases such as MDM2 [1]. In the last decade, diverse physiological functions of p53 have been reported. Regulation of metabolic pathways such as glycolysis, oxidative phosphorylation, and fatty acid oxidation are among these functions of p53 [2]. Furthermore it has been shown that p53 regulates mitochondrial function, which is closely involved in metabolic regulation [3,4]. An important regulatory system of mitochondrial function is mitochondrial biogenesis. In most cases, mitochondrial biogenesis is organized by a transcriptional coactivator PGC1α, which is a protein product of *Ppargc1a* and upregulates nuclear genes encoding mitochondrial proteins via enhancement of mRNA expression of transcriptional factors such as NRF1 and NRF2 [5]. It has been reported previously that p53 positively or negatively regulates *Ppargc1a* expression according to each tissue or cell type [6–9]. Furthermore, it has been reported that p53 deficient fibroblasts show low mtDNA copy number [10], and p53 accumulation in neonatal cardiomyocytes leads to mitochondrial impairment [8]. Thus, although there are emerging evidences for links between p53 and mitochondrial biogenesis, the distinct physiological roles in each tissue type remain unclear.

Control of cell differentiation is also regarded as one of the diverse physiological functions of p53. For example, it was recently

* Corresponding authors at: Department of Internal Medicine Research, Sasaki Institute, Sasaki Foundation, 2-2 Kandasurugadai, Chiyoda-ku, Tokyo 101-0062, Japan (N. Okita), Laboratory of Molecular Pathology and Metabolic Disease, Faculty of Pharmaceutical Sciences, Tokyo University of Science, 2641 Yamazaki, Noda-shi, Chiba 278-0022, Japan (Y. Higami).
E-mail addresses: okita@po.kyoundo.jp, nmsokita@gmail.com (N. Okita), higami@rs.noda.tus.ac.jp (Y. Higam).
[1] These authors contributed equally to this work.

http://dx.doi.org/10.1016/j.bbrc.2014.02.059
0006-291X/

reported that in the process of reprogramming differentiated cells into induced pluripotent stem cells, p53 functions as a barrier to dedifferentiation [11]. Also, in the field of cell differentiation, roles for p53 in adipogenesis and myogenesis have been reported. mouse embryonic fibroblasts (MEFs) or bone marrow-derived mesenchymal stem cells (MSCs) derived from p53 knockout (KO) mice and p53 knockdown 3T3-L1 preadipocytes differentiate into adipocytes more efficiently than p53 proficient cells [12–14]. In C2C12 myoblasts p53 knockdown or p53 mutant expression inhibits its differentiation to myotubes [12,15,16]. Thus, the roles of p53 in cell differentiation differ according to cell types.

Investigation of individual tissues involved in energy metabolism appeared to be important to elucidate the diversity of the metabolic roles of p53 in energy metabolism within the whole body. Therefore in this study, we selected adipose tissue and skeletal muscle, which are peripheral metabolic tissues, as the target tissues. Adipose tissue, which is mainly composed of adipocytes, functions as an organ for energy storage and release *via* lipid metabolism. Skeletal muscle, which is mainly composed of myotubes, plays a central role for basal metabolism in the whole body. Using 3T3-L1 preadipocytes and MEFs as the origin cells of adipocytes and C2C12 myoblasts as the origin cells of myotubes, we found that p53 has a differential contribution to mitochondrial biogenesis and cell differentiation in each cell type. Our results imply that p53 is a key factor that reflects on tissue-specific diversity in metabolism.

2. Materials and methods

2.1. Cell lines and drugs

3T3-L1 preadipocytes were purchased from RIKEN Bioresource Center (Ibaraki, Japan) and 3T3-L1/shGFP and 3T3-L1/shp53 preadipocytes were previously established by our laboratory using a retrovirus system [17,18]. Primary mouse embryonic fibroblasts (MEFs) derived from p53 WT and p53 KO mice (RIKEN Bioresource Center) were established as previously reported by our laboratory [19]. C2C12 myoblasts were kindly provided by Dr. Kazuhiro Shigemoto. C2C12/shGFP and C2C12/shp53 myoblasts were established as the same retroviral systems used for 3T3-L1/shGFP and 3T3-L1/shp53. Nutlin-3a was supplied by Cayman (MI, USA).

2.2. Cell culture and differentiation

3T3-L1 preadipocytes were maintained in DMEM (low glucose) (Wako Pure Chemical; Osaka, Japan) with 10% fetal calf serum (FCS) (Bovogen Biologicals; Victoria, Australia) and 1% penicillin/streptomycin (Sigma; MO, USA). MEFs were grown in DMEM (high glucose) (Wako Pure Chemical) with 10% FCS, 0.1 mM 2-mercaptoethanol, and 1% penicillin/streptomycin. Differentiation of 3T3-L1 preadipocytes or MEFs to adipocytes was performed as previously reported by our laboratory [18]. C2C12 myoblasts were maintained in DMEM high glucose supplemented with 10% FCS and antibiotics. Differentiation of C2C12 myoblasts to myotubes was performed using horse serum essentially as previously reported [20].

2.3. Western blotting

Western blotting was performed as previously reported by our laboratory [18,19,21] with the following primary antibodies: anti-p53 monoclonal antibody (clone Ab-1; Calbiochem; CA, USA), anti-β actin monoclonal antibody (clone AC-15; Sigma), or anti-α tubulin monoclonal antibody (clone DM1A; Sigma), anti-PPARγ polyclonal antibody (E-8; Santa Cruz Biotechnology; CA, USA), anti-FABP4 polyclonal antibody (Cayman), anti-COXIV polyclonal antibody (Cell Signaling Technology; MA USA), anti-TOM20 (clone 4S3; Sigma).

2.4. Oil Red O staining

Oil Red O staining was performed as previously reported by our laboratory [18,19]. The stained cells were observed by a BIOREVO BZ-9000 microscope (Keyence; Osaka, Japan).

2.5. RNA purification and RT-PCR

RNA purification and RT-PCR were performed essentially as previously reported by our laboratory [19,21]. Total RNA was extracted from cells using RNAiso PLUS (TaKaRa; Shiga, Japan) and purified with a FastPure RNA kit (TaKaRa) according to the manufacturer's protocol. The purified RNA was subjected to reverse transcription with PrimeScript Reverse Transcriptase (TaKaRa) and random hexamer (TaKaRa). The semi-quantitative RT-PCR was performed using Platinum Taq DNA Polymerase High Fidelity (Invitrogen). Quantitative RT-PCR was performed using the Applied Biosystems 7300 real-time PCR system (Applied Biosystems; CA, USA) and SYBR Premix Ex Taq II (TaKaRa) according to the manufacturer's protocol. The sequences of primers used for RT-PCR are shown in Table 1.

2.6. Mitochondrial DNA (mtDNA) content

mtDNA content was evaluated essentially as previously reported by our laboratory [21]. Briefly, extracted total DNA was subjected to real-time PCR using COXII primers (forward, 5′-CCATCCCAGGCCGACTAA-3′; reverse, 5′-AATTTCAGAGCATTGGCCATAGA-3′) or β-Globin primers (forward, 5′-ATCCAGGTTACAAGGCAGCT-3′; reverse, 5′-GGGAAACATAGACAGGGG-3′). The relative mitochondrial copy number is represented by the ratio of COXII encoded in mtDNA to β-Globin encoded in genomic DNA.

2.7. Citrate synthase (CS) and Complex IV activity

To prepare cell lysates for the measurement of mitochondrial activity, 3T3-L1/shGFP and 3T3-L1/shp53 were homogenized in homogenization buffer containing 50 mM Tris–HCl, pH 7.4, 150 mM NaCl, 1% phosphatase inhibitor cocktail, 5 mM EDTA, 1% protease inhibitor cocktail, 1% NP-40 and 0.05% sodium deoxycholate. Protein concentration was determined using the BCA protein assay kit (Thermo Scientific; IL, USA) according to the manufacturer's protocol.

CS activity was measured by monitoring color development of thio-bis-(2-nitrobenzoic) acid (TNB) generated from reduction of 5,5-dithio-bis-(2-nitrobenzoic) acid (DTNB) by CoA-SH, the by-product of citrate, as previously reported [21]. Briefly, cell lysates were added to reaction mixtures containing 0.1 mM DTNB, 0.5 mM acetyl-CoA, 0.1% Triton X-100 and 100 mM Tris–HCl, pH 8.0. After incubation at 25 °C for 5 min, reactions were then initiated by the addition of 0.5 mM oxaloacetate in a final volume of 200 μL, and the change in absorbance at 412 nm was recorded for at least 3 min using ARVO MX/Light Wallac 1420 Multilabel/Luminescence Counter (PerkinElmer; MA, USA).

Complex IV activity was measured by monitoring the change in absorbance at 550 nm of cytochrome *c* by oxidation as previously reported [21]. Briefly, reactions were initiated by adding cell homogenates to the reaction mixture containing 50 mM Tris–HCl, pH 7.2, and 25 μM reduced cytochrome *c*. The absorbance at 550 nm (at 30 °C) was measured using EnVision Multilabel Reader (PerkinElmer). The first order rate constant (k) was calculated from

Table 1
Sequences of primers used in RT-PCR.

Gene	Forward sequence	Reverse sequence
Actb	5′-TCTTTGCAGCTCCTTCGTTG-3′	5′-GGCCTCGTCACCCACATAG-3′
Fabp4	5′-TCGATGATTACATGAAAGAAGTGG-3′	5′-CGCCCAGTTTGAAGGAAATC-3′
Gusb	5′-CCAGAGCGAGTATGGAGCAGAC-3′	5′-GGTGACTGGTTCGTCATGAAGTC-3′
Myod	5′-CTGCTCTGATGGCATGATGG-3′	5′-TATGCTGGACAGGCAGTCG-3′
Myog	5′-ATCCAGTACATTGAGCGCCTAC-3′	5′-TGTCCACGATGGACGTAAGG-3′
p21	5′- AGTACTTCCTCTGCCCTGCTG -3′	5′-GCGCTTGGAGTGATAGAAATCTG-3′
p53	5′-TAAAGGATGCCCATGCTACAG-3′	5′-GACCGGGAGGATTGTGTCTC-3′
Pgc1a	5′-AGACGGATTGCCCTCATTTG-3′	5′-CAGGGTTTGTTCTGATCCTGTG-3′
Pparg	5′-CACAATGCCATCAGGTTTGG-3′	5′-GCGGGAAGGACTTTATGTATGAG-3′
Rps18	5′-TGCGAGTACTCAACACCAACAT-3′	5′-CTTTCCTCAACACCACATGAGC-3′
Tbp	5′-CAGTACAGCAATCAACATCTCAGC-3′	5′-CAAGTTTACAGCCAAGATTCACG-3′

the natural logarithms of the absorbance after the addition of cell homogenates.

2.8. Statistical analysis

All statistical analyses (Student's *t*-test with or without Bonferroni correction) were performed using R software (R project for Statistical Computing). Differences with p values <0.05 were deemed statistically significant.

3. Results

3.1. Distinct effects of p53 on Ppargc1a expression in 3T3-L1 preadipocytes and C2C12 myoblasts

By using Nutlin-3a, which is a chemical inhibitor of MDM2 E3 ligase [22,23], when examining metabolic regulation by DNA damage-independent p53 stabilization in adipocytes and myotubes, we obtained interesting results. In both C2C12 myoblasts (Fig. 1A, left panel) and 3T3-L1 preadipocytes (Fig. 1B, left panel) Nutlin-3a induced p53 protein accumulation and p21 mRNA expression in a dose dependent manner. Interestingly, in 3T3-L1 preadipocytes (Fig. 1B, right panel) but not in C2C12 myotubes (Fig. 1A, right panel), *Ppargc1a* expression was decreased in a dose dependent manner. To exclude side-effects of Nutlin-3a, we examined whether p53 exogenous overexpression decreases *Ppargc1a* expression. Consistent with Nutlin-3a treatment, p53 overexpression in 3T3-L1 preadipocytes (Fig. 1D) but not C2C12 myoblasts (Fig. 1C) reduced *Ppargc1a* expression significantly. Next, to investigate the effects of p53 downregulation on *Ppargc1a* expression, we used p53-knockdown (KD) C2C12 myoblasts and 3T3-L1 preadipocytes (Fig. 1E and F, left panel). As shown in Fig. 1E and F, no significant change of *Ppargc1a* expression occurred in either of the cell lines. In these experimental conditions, although we analyzed the protein levels of PGC1α, a protein product of *Ppargc1a*, by Western blotting using two commercially available anti-PGC1α antibodies (Santa Cruz Biotechnology, Cat. No. sc-13067 and Merk-Millipore, Cat. No. ST1202-1SET), we were not, unfortunately, able to detect any specific signals (data not shown). These results indicate that, p53 up-regulation in 3T3-L1 preadipocytes but not C2C12 myoblasts reduces *Ppargc1a* expression.

3.2. Effects of p53 downregulation on Ppargc1a expression and mtDNA content in myotubes differentiated from C2C12 myoblasts

Previous studies have suggested that p53 plays a positive regulatory role in mitochondrial regulation in skeletal muscle and myotubes [6,24]. However, our data indicated that, at least in C2C12 myoblasts, which were established from skeletal muscle [25], p53 may play an opposing role (Fig. 1). We therefore sought to investigate the involvement of p53 in mitochondrial regulation in myotubes differentiated from myoblasts (Fig. 2). Several studies have shown that p53 positively regulates differentiation of C2C12 myoblasts into myotubes [12,15,16]. Consistent with the previous studies, p53 knockdown inhibited multinucleated myotube formation slightly (Fig. 2A) and tended to reduce the mRNA expression of differentiation markers (*Myog* and *Myod*) during myogenesis compared with control cells (data not shown). Interestingly, we found that *Ppargc1a* expression (Fig. 2B) and mtDNA content (Fig. 2C) were not affected by p53 downregulation, even in myotubes. These results indicate that p53 does not affect mitochondrial regulation in myotubes, although differentiation of C2C12 myoblasts to myotubes is suppressed by p53 knockdown.

3.3. Effects of p53 downregulation on Ppargc1a expression and mtDNA content in adipocytes derived from 3T3-L1 preadipocytes and MEFs

As shown in Fig. 1, it seemed to suggest that p53 is a negative regulator of mitochondrial biogenesis in 3T3-L1 preadipocytes. Because previous studies have reported that mitochondrial biogenesis is upregulated during adipogenesis of 3T3-L1 preadipocytes [26,27], we sought to confirm the effects of p53 knockdown on signs of mitochondrial biogenesis during adipogenesis. The results of Oil Red O staining showed that p53 KD leads to efficient accumulation of lipid droplets (Fig. 3A). Consistent with this result, the mRNA expressions of adipogenesis markers (*Pparg and Fabp4*) during differentiation of 3T3-L1/shp53 preadipocytes to adipocytes tended to increase compared with control (data not shown). Similar to the result in preadipocytes (Fig. 1), we found that p53-knockdown mature adipocytes have significantly increased *Ppargc1a* expression (Fig. 3B). Interestingly, since Day 8, mtDNA content in p53-knockdown cells significantly increased compared with those in mock cells (Fig. 3C). Furthermore we quantitatively analyzed protein levels of PPARγ2 (a form of PPARγ protein responsible for adipogenesis) [28] and FABP4, which are protein products of *Pparg* and *Fabp4*, respectively. As shown in Fig. 3D, the protein levels of both PPARγ2 and FABP4 in 3T3-L1/shp53 cells at Day 8 of adipocyte differentiation are significantly higher than in the control. These results are consistent with a previous finding that p53 downregulation promotes adipogenesis in 3T3-L1 preadipocytes [14]. Since p53 downregulation in 3T3-L1 adipocyte-committed cells leads to the enhancement of adipogenesis and increase in mtDNA content, we analyzed whether the similar results were obtained in p53-deficient MEFs, adipocyte-uncommitted cells. Primary MEFs from p53 WT mice and p53 KO mice were differentiated into adipocytes. Oil Red O staining of the differentiated MEFs revealed that adipocytes from p53 KO MEFs accumulated more lipid droplets compared with those from p53 WT MEFs (Fig. 3E). Furthermore, as shown in Supplemental Fig. 1, the mRNA levels of adipocyte differentiation

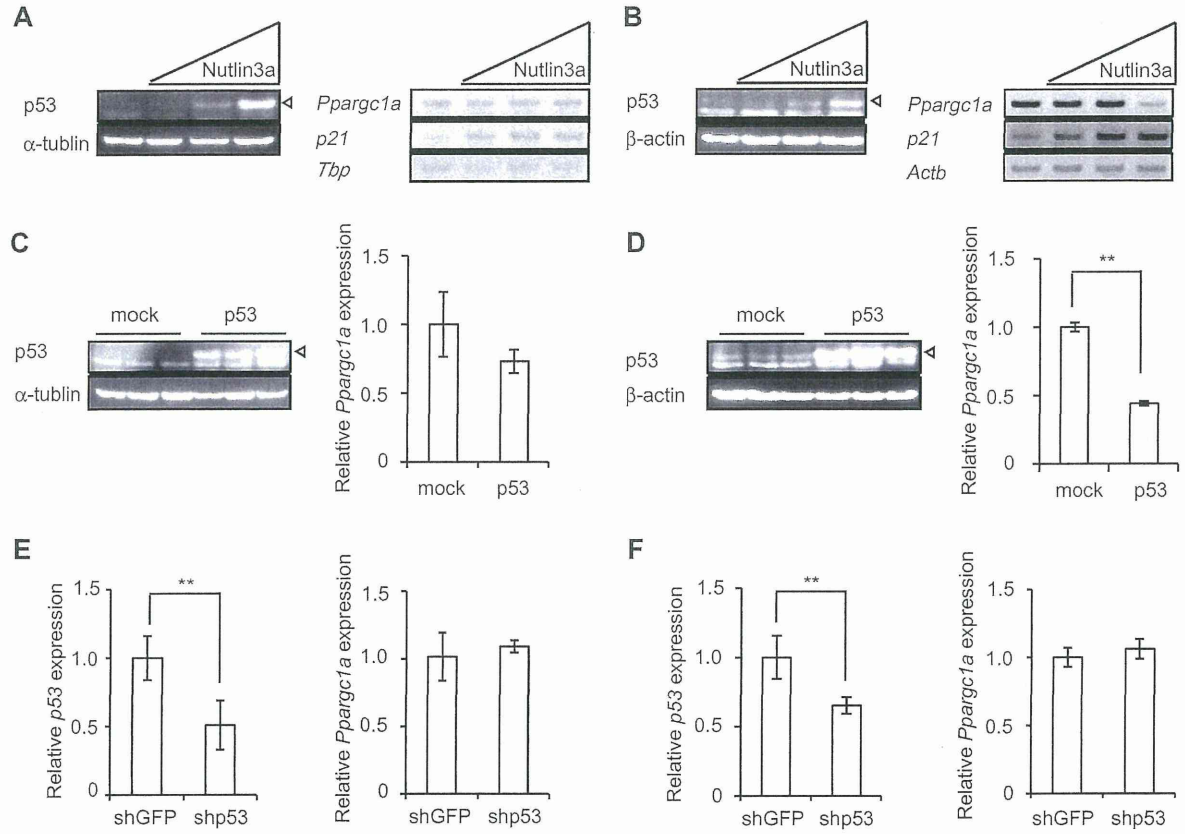

Fig. 1. Differential impacts of p53 on *Ppargc1a* expression in myoblasts and preadipocytes. (A, B) C2C12 myoblasts (A) and 3T3-L1 preadipocytes (B) were treated with 0, 1, 5, or 25 μM of Nutlin3a for 24 h. Protein levels of p53 were analyzed by Western blotting (left panels). Open triangles indicate the signals from p53. α-Tubulin (for C2C12 cells) or β-actin (3T3-L1 cells) was used as a loading control. *Ppargc1a* and *p21* expression levels were analyzed by RT-PCR (right panels). *Tbp* (for C2C12 cells) or *Actb* (for 3T3-L1 cells) was used as a loading control. (C, D) C2C12 myoblasts (C) and 3T3-L1 preadipocytes (D) were transfected with mouse p53 expression (exo-p53) or empty vector (mock). The cells were harvested after 20 h of transfection. Protein levels of p53 were analyzed by Western blotting (left panels). α-Tubulin (C; for C2C12 cells) or β-actin (D; for 3T3-L1 cells) was used as a loading control. (E, F) C2C12 myoblasts (E) and 3T3-L1 preadipocytes (F) were stably transfected with either p53 (shp53) or GFP (shGFP) shRNA expression vectors. *p53* and *Ppargc1a* expression levels were analyzed by quantitative real-time PCR. *Tbp* (E; for C2C12 cells) or *Rps18* (F; for 3T3-L1 cells) was used as a loading control. The quantitative data are represented as means ± SD ($n = 3$) (**$p < 0.01$).

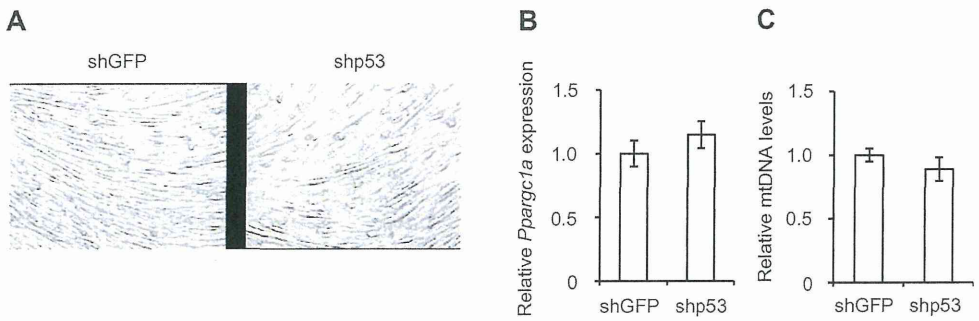

Fig. 2. Effects of p53 downregulation on *Ppargc1a* expression and mtDNA content in myotubes differentiated from C2C12 myoblasts. p53-knockdown (shp53) and control (shGFP) C2C12 myoblasts were differentiated into myotubes (Day 5) and the pictures were taken using a phase contrast microscope (magnification; ×200) (A). *Ppargc1a* expression (B) and mtDNA content (C) in myoblasts (Day 5) were analyzed by quantitative real-time PCR. *Tbp* was used as a reference control. All data reported (means ± SD) were not statistically significant ($n = 3$).

markers appeared to be moderately higher in p53KO MEFs than in p53 WT MEFs. These results were consistent with previously reported findings [12,13]. Next, we examined the effects of p53 on *Ppargc1a* expression and mtDNA content in adipocytes from MEFs using this adipogenesis system. Both the contents of mtDNA and *Ppargc1a* expression in adipocytes at Day16 after differentiation induction increased in p53 KO adipocytes compared with p53 WT adipocytes (Fig. 3F and G). Next, we investigated quantity of proteins that constitute mitochondrion. As shown in Fig. 3H, COX4, a subunit of mitochondrial cytochrome oxidase complex, and TOM20, a subunit of mitochondrial import receptor, increased in p53-knockdown adipocytes compared with control adipocytes.

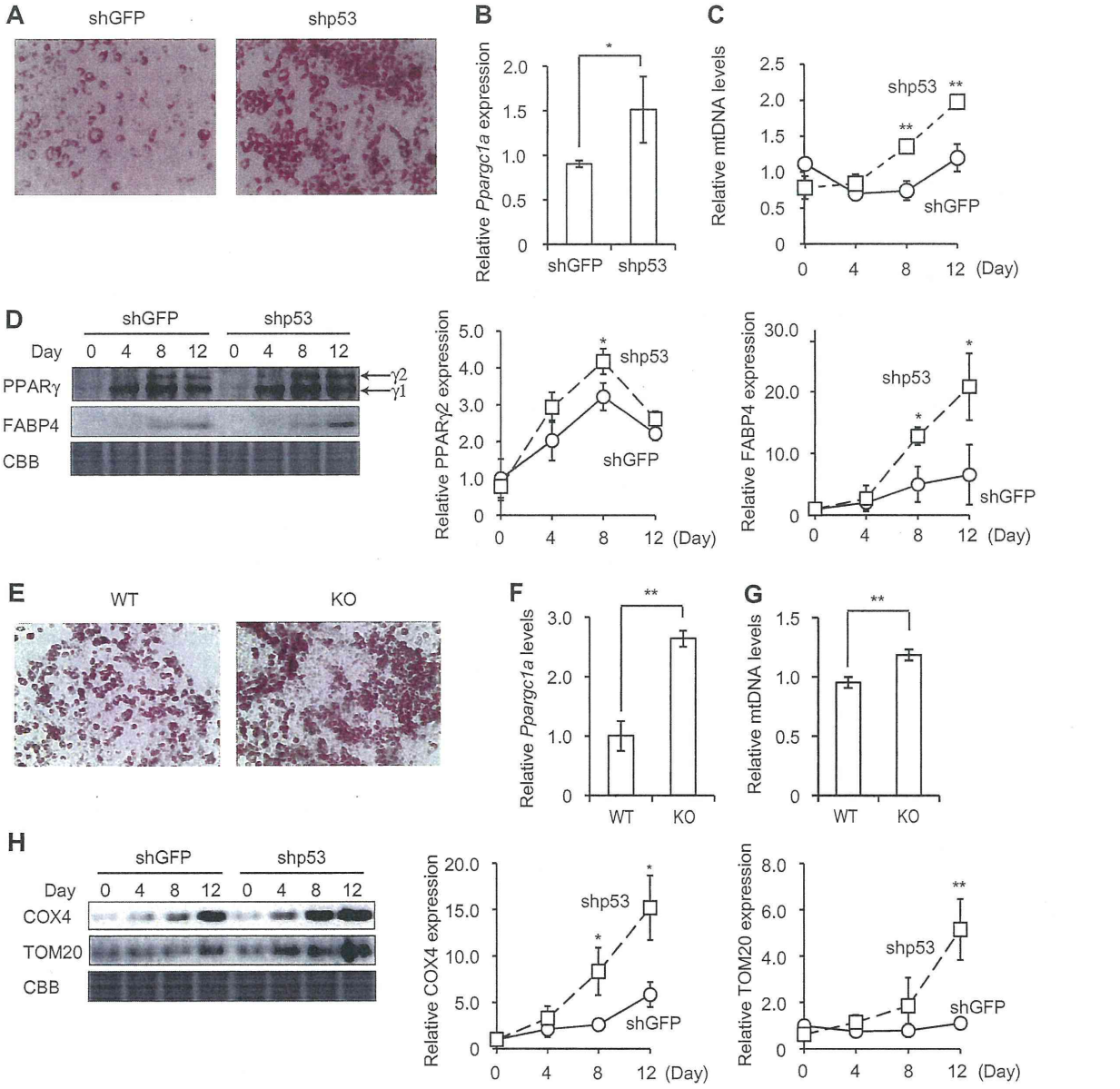

Fig. 3. Effects of p53 downregulation on *Ppargc1a* expression and mtDNA content in adipocytes derived from 3T3-L1 preadipocytes and MEFs. (A) shRNA-mediated p53-knockdown (shp53) and control (shGFP) 3T3-L1 preadipocytes were differentiated into adipocytes (Day 12) and stained with Oil Red O to observe intracellular triglyceride accumulation. (B) *Ppargc1a* expression in adipocytes (Day 12) was analyzed by quantitative real-time PCR. *Rps18* was used as a reference control. (C) Mitochondrial DNAs purified from differentiated adipocytes were analyzed by quantitative real-time PCR. (D) Extracted proteins from each day were subjected to Western blotting with the indicated antibodies. Representative images and the quantitative data ($n = 3$) were shown. CBB staining was used as a loading control. (E) p53 WT and p53 KO MEFs were differentiated to adipocytes (Day 16), and stained with Oil Red O to observe intracellular triglyceride accumulation ($n = 4$). (F, G) *Ppargc1a* expression (F) and mtDNA content (G) in adipocytes (Day 16) were analyzed by quantitative real-time PCR ($n = 3$). *Gusb* was used as a reference control. (H) Extracted proteins from each day were subjected to Western blotting with the indicated antibodies. Representative images and the quantitative data ($n = 3$) were shown. The quantitative data are represented as means ± SD ($n = 3$–5) (*$p < 0.05$; **$p < 0.01$).

These results suggest that p53 affects on mitochondrial content during adipogenesis.

3.4. Effects of p53 downregulation on mitochondrial metabolic function during adipogenesis

Since Fig. 3 showed that p53 downregulation increases mitochondrial content during adipogenesis, we investigated whether the mitochondrial activity increases consistent with the observation. For this purpose, we selected two enzyme activities involved in metabolic pathway existed in mitochondria. As shown in Fig. 4, both CS, a member of TCA cycle, and Complex IV, a member of electron transport chain, activity in p53-knockdown adipocytes significantly increased compared with those in mock cells.

4. Discussion

In the present study, on the ground of increases in mtDNA content and mitochondrial protein accompanying mitochondrial metabolic activity, we demonstrated that p53 is a negative regulator of mitochondrial biogenesis in adipocytes, which is one of peripheral tissues important in energy metabolism. On the other hand, we

have also considered mitochondrial elimination systems during adipogenesis. Autophagy is one of the most important systems for mitochondrial turn-over [29]. Recently our group has reported that autophagosomes accumulate in a p53-independent manner during adipogenesis [18] and anticipate that this phenomenon would result in impairment of autophagy during adipogenesis. Hence, our observation in this study, that p53 possesses an inhibitory effect on mitochondrial content in adipocyte lineage, is unlikely to be related to autophagy-mediated mitochondrial elimination.

By using C2C12 myoblasts, which are derived from skeletal leg muscle of a C3H mouse [30], we also confirmed the contribution of p53 to mitochondrial biogenesis. However, our results showed that p53 did not dramatically affect *Ppargc1a* expression and mtDNA content in C2C12 myoblasts and myotubes (Figs. 1 and 2). In the past, the relationship between p53 and mitochondrial regulation in skeletal muscle has been examined and characterized. *Ppargc1a* expression and mtDNA content of the skeletal muscle of p53 null mice are reduced in comparison with those of WT mice [6,24]. Furthermore, the effects of p53 on mitochondrial biogenesis were greater for slow twitch fiber-rich muscles versus fast twitch fiber-rich muscles [24]. Taken together with the past findings, this finding may imply that C2C12 cells possess features of fast twitch fiber-rich muscle.

What is the molecular mechanism of p53-mediated mitochondrial regulation in adipocyte lineage? This important question may be able to explain by PGC1α-orchestrated mitochondrial biogenesis. The past findings have indicated about two sides of p53-mediated PGC1α regulation [6–9]. Our present study demonstrated that, at least in adipocyte lineage (preadipocyte and mature adipocyte), p53 functions as a negative regulator of *Ppargc1a*. Although it is important to confirm the changes of the protein levels of PGC1α, we were not able to detect endogenous PGC1α protein under any experimental conditions performed in this study. Generally the protein level of PGC1α is very low in white adipose tissue and, even in brown adipose tissue, in which the protein level of PGC1α is relatively high, stimuli such as cold shock is required for the specific detection of PGC1α protein by Western blotting [31,32]. Nevertheless, the study of adipose tissue-specific *Ppargc1a*-disrupted mice revealed evidence that, in the absence of such stimuli, *Ppargc1a* is involved in fatty acid oxidation and tricarboxylic acid cycle in white adipose tissue [32]. This fact implies that the basal expression of *Ppargc1a* can contribute to physiological functions in adipocytes.

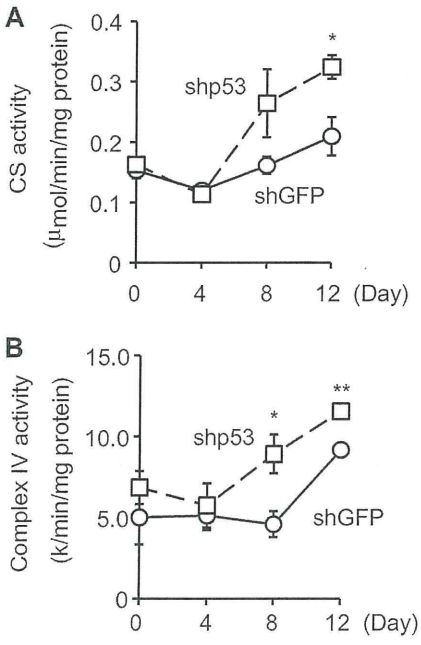

Fig. 4. Effects of p53 downregulation on mitochondrial metabolic function during adipogenesis. CS (A) and Complex IV (B) activities were analyzed as described in Section 2. The quantitative data are represented as means ± SD ($n = 3$) (*$p < 0.05$; **$p < 0.01$).

In this study, we showed that in muscle cells p53 promotes differentiation of C2C12 myoblasts into myotubes, but does not influence mitochondrial biogenesis, whereas in adipocytes p53 inhibits adipogenesis and plays a negative regulatory role in mitochondrial regulation. Recent *in vivo* studies demonstrated the negative effects of p53 on whole body metabolism via adipose tissue, and that adipose tissue-specific p53 depletion suppressed aging and inflammation, and improved insulin sensitivity [33]. Furthermore, mitochondrial content or quality is closely involved in insulin sensitivity [34]. Thus, our *in vitro* study in regard to adipocytes provides evidence of these *in vivo* results.

Acknowledgments

We thank Drs. Toshio Kitamura (The University of Tokyo, Japan) and Kazuhiro Shigemoto (Tokyo Metropolitan Institute of Gerontology, Japan) for provision of the research materials; Dr. Takao Sekiya (Sasaki Foundation, Japan) for his cooperation. The authors also thank all members of Laboratory of Molecular Pathology and Metabolic Disease for their encouragements. This work was partially supported by a Grant-in-Aid for Young Scientists (B) (23790201 and 25860759, N.O.) and for Challenging Exploratory Research (23659207, Y.H.) from the Japan Society for the Promotion of Science.

Appendix A. Supplementary data

Supplementary data associated with this article can be found, in the online version, at http://dx.doi.org/10.1016/j.bbrc.2014.02.059.

References

[1] J.P. Kruse, W. Gu, Modes of p53 regulation, Cell 137 (2009) 609–622.
[2] O.D. Maddocks, K.H. Vousden, Metabolic regulation by p53, J. Mol. Med. (Berl.) 89 (2011) 237–245.
[3] A. Saleem, H.N. Carter, S. Iqbal, et al., Role of p53 within the regulatory network controlling muscle mitochondrial biogenesis, Exerc. Sport Sci. Rev. 39 (2011) 199–205.
[4] P.Y. Wang, J. Zhuang, P.M. Hwang, P53: exercise capacity and metabolism, Curr. Opin. Oncol. 24 (2012) 76–82.
[5] D.P. Kelly, R.C. Scarpulla, Transcriptional regulatory circuits controlling mitochondrial biogenesis and function, Genes Dev. 18 (2004) 357–368.
[6] A. Saleem, P.J. Adhihetty, D.A. Hood, Role of p53 in mitochondrial biogenesis and apoptosis in skeletal muscle, Physiol. Genomics 37 (2009) 58–66.
[7] E. Sahin, S. Colla, M. Liesa, et al., Telomere dysfunction induces metabolic and mitochondrial compromise, Nature 470 (2011) 359–365.
[8] C. Villeneuve, C. Guilbeau-Frugier, P. Sicard, et al., P53-PGC-1alpha pathway mediates oxidative mitochondrial damage and cardiomyocyte necrosis induced by monoamine oxidase-A upregulation: role in chronic left ventricular dysfunction in mice, Antioxid. Redox Signal. 18 (2013) 5–18.
[9] K. Aquilano, S. Baldelli, B. Pagliei, et al., P53 orchestrates the PGC-1a-mediated antioxidant response upon mild redox and metabolic imbalance, Antioxid. Redox Signal. 18 (2013) 386–399.
[10] M.A. Lebedeva, J. Eaton, G.S. Shadel, Loss of p53 causes mitochondrial DNA depletion and altered mitochondrial reactive oxygen species homeostasis, Biochim. Biophys. Acta 1787 (2009) 328–334.
[11] L. Yi, C. Lu, W. Hu, et al., Multiple roles of p53 related pathways in somatic cell reprogramming and stem cell differentiation, Cancer Res. 72 (2012) 5635–5645.
[12] A. Molchadsky, I. Shats, N. Goldfinger, et al., P53 plays a role in mesenchymal differentiation programs, in a cell fate dependent manner, PLoS One 3 (2008) e3707.
[13] A. Armesilla-Diaz, G. Elvira, A. Silva, P53 regulates the proliferation, differentiation and spontaneous transformation of mesenchymal stem cells, Exp. Cell Res. 315 (2009) 3598–3610.

[14] A. Molchadsky, O. Ezra, P.G. Amendola, et al., P53 is required for brown adipogenic differentiation and has a protective role against diet-induced obesity, Cell Death Differ. 20 (2013) 774–783.
[15] Y. Tamir, E. Bengal, P53 protein is activated during muscle differentiation and participates with MyoD in the transcription of muscle creatine kinase gene, Oncogene 17 (1998) 347–356.
[16] A. Porrello, M.A. Cerone, S. Coen, et al., P53 regulates myogenesis by triggering the differentiation activity of pRb, J. Cell Biol. 151 (2000) 1295–1304.
[17] S. Morita, T. Kojima, T. Kitamura, Plat-E: an efficient and stable system for transient packaging of retroviruses, Gene Ther. 7 (2000) 1063–1066.
[18] K. Mikami, N. Okita, Y. Tokunaga, et al., Autophagosomes accumulate in differentiated and hypertrophic adipocytes in a p53-independent manner, Biochem. Biophys. Res. Commun. 427 (2012) 758–763.
[19] S. Matsushima, N. Okita, M. Oku, et al., An Mdm2 antagonist, Nutlin-3a, induces p53-dependent and proteasome-mediated poly(ADP-ribose) polymerase1 degradation in mouse fibroblasts, Biochem. Biophys. Res. Commun. 407 (2011) 557–561.
[20] S. Mori, S. Kubo, T. Akiyoshi, et al., Antibodies against muscle-specific kinase impair both presynaptic and postsynaptic functions in a murine model of myasthenia gravis, Am. J. Pathol. 180 (2012) 798–810.
[21] N. Okita, Y. Hayashida, Y. Kojima, et al., Differential responses of white adipose tissue and brown adipose tissue to caloric restriction in rats, Mech. Ageing Dev. 133 (2012) 255–266.
[22] L.T. Vassilev, B.T. Vu, B. Graves, et al., In vivo activation of the p53 pathway by small-molecule antagonists of MDM2, Science 303 (2004) 844–848.
[23] T. Thompson, C. Tovar, H. Yang, et al., Phosphorylation of p53 on key serines is dispensable for transcriptional activation and apoptosis, J. Biol. Chem. 279 (2004) 53015–53022.
[24] J.Y. Park, P.Y. Wang, T. Matsumoto, et al., P53 improves aerobic exercise capacity and augments skeletal muscle mitochondrial DNA content, Circ. Res. 105 (2009) 705–712.
[25] H.M. Blau, C.P. Chiu, C. Webster, Cytoplasmic activation of human nuclear genes in stable Heterocaryons, Cell 32 (1983) 1171–1180.
[26] L. Wilson-Fritch, A. Burkart, G. Bell, et al., Mitochondrial biogenesis and remodeling during adipogenesis and in response to the insulin sensitizer rosiglitazone, Mol. Cell. Biol. 23 (2003) 1085–1094.
[27] S. Vankoningsloo, M. Piens, C. Lecocq, et al., Mitochondrial dysfunction induces triglyceride accumulation in 3T3-L1 cells: role of fatty acid beta-oxidation and glucose, J. Lipid Res. 46 (2005) 1133–1149.
[28] P. Tontonoz, E. Hu, B.M. Spiegelman, Stimulation of adipogenesis in fibroblasts by PPAR gamma 2, a lipid-activated transcription factor, Cell 79 (1994) 1147–1156.
[29] I. Kim, S. Rodriguez-Enriquez, J.J. Lemasters, Selective degradation of mitochondria by Mitophagy, Arch. Biochem. Biophys. 462 (2007) 245–253.
[30] D. Yaffe, O. Saxel, Serial passaging and differentiation of myogenic cells isolated from dystrophic mouse muscle, Nature 270 (1977) 725–727.
[31] P. Puigserver, Z. Wu, C.W. Park, et al., A cold-inducible coactivator of nuclear receptors linked to adaptive thermogenesis, Cell 92 (1998) 829–839.
[32] S. Kleiner, R.J. Mepani, D. Laznik, et al., Development of insulin resistance in mice lacking PGC-1α in adipose tissues, Proc. Natl. Acad. Sci. U.S.A. 109 (2012) 9635–9640.
[33] T. Minamino, M. Orimo, I. Shimizu, et al., A crucial role for adipose tissue p53 in the regulation of insulin resistance, Nat. Med. 15 (2009) 1082–1087.
[34] Z. Cheng, Y. Tseng, M.F. White, Insulin signaling meets mitochondria in metabolism, Trends Endocrinol. Metab. 21 (2010) 589–598.

Am J Physiol Gastrointest Liver Physiol 304: G428–G436, 2013.
First published December 28, 2012; doi:10.1152/ajpgi.00356.2012.

Epithelial transient receptor potential ankyrin 1 (TRPA1)-dependent adrenomedullin upregulates blood flow in rat small intestine

Toru Kono,[1,2] Atsushi Kaneko,[2,3] Yuji Omiya,[2,3] Katsuya Ohbuchi,[3] Nagisa Ohno,[3] and Masahiro Yamamoto[3]

[1]Center for Clinical and Biomedical Research, Sapporo Hisgashi Tokushukai Hospital, Hokkaido, Japan; [2]Division of Gastroenterologic and General Surgery, Department of Surgery, Asahikawa Medical University, Hokkaido, Japan; and [3]Tsumura Research Laboratories, Tsumura and Co., Ibaraki, Japan.

Submitted 10 September 2012; accepted in final form 19 December 2012

Kono T, Kaneko A, Omiya Y, Ohbuchi K, Ohno N, Yamamoto M. Epithelial transient receptor potential ankyrin 1 (TRPA1)-dependent adrenomedullin upregulates blood flow in rat small intestine. *Am J Physiol Gastrointest Liver Physiol* 304: G428–G436, 2013. First published December 28, 2012; doi:10.1152/ajpgi.00356.2012.—The functional roles of transient receptor potential (TRP) channels in the gastrointestinal tract have garnered considerable attention in recent years. We previously reported that daikenchuto (TU-100), a traditional Japanese herbal medicine, increased intestinal blood flow (IBF) via adrenomedullin (ADM) release from intestinal epithelial (IE) cells (Kono T et al. *J Crohns Colitis* 4: 161–170, 2010). TU-100 contains multiple TRP activators. In the present study, therefore, we examined the involvement of TRP channels in the ADM-mediated vasodilatatory effect of TU-100. Rats were treated intraduodenally with the TRP vanilloid type 1 (TRPV1) agonist capsaicin (CAP), the TRP ankyrin 1 (TRPA1) agonist allyl-isothiocyanate (AITC), or TU-100, and jejunum IBF was evaluated using laser-Doppler blood flowmetry. All three compounds resulted in vasodilatation, and the vasodilatory effect of TU-100 was abolished by a TRPA1 antagonist but not by a TRPV1 antagonist. Vasodilatation induced by AITC and TU-100 was abrogated by anti-ADM antibody treatment. RT-PCR and flow cytometry revealed that an IEC-6 cell line originated from the small intestine and purified IE cells expressed ADM and TRPA1 but not TRPV1. AITC increased ADM release in IEC cells remarkably, while CAP had no effect. TU-100 and its ingredient 6-shogaol (6SG) increased ADM release dose-dependently, and the effects were abrogated by a TRPA1 antagonist. 6SG showed similar TRPA1-dependent vasodilatation in vivo. These results indicate that TRPA1 in IE cells may play an important role in controlling bowel microcirculation via ADM release. Epithelial TRPA1 appears to be a promising target for the development of novel strategies for the treatment of various gastrointestinal disorders.

daikenchuto; TU-100; vasodilatation; 6-shogaol; inflammatory bowel diseases

TRANSIENT RECEPTOR POTENTIAL (TRP) channels are nonselective calcium ion channels ubiquitously expressed in many tissues and are known to participate in a broad range of physical, chemical, and environmental stimuli such as taste, temperature, changes in osmolarity, pressure, stretch, and light.

TRP channels are divided into seven subfamilies with 27 different channel types present in humans. Natural products, especially medicinal and culinary herbs such as chili pepper, mustard oil, and menthol, are known to stimulate some of these TRP channels. In recent years there has been a growing interest in elucidating the role of TRP channels in gastrointestinal physiology, including intestinal motility, secretion, and visceral sensation (23, 24, 39, 53). However, the physiological implications of TRP channels in intestinal blood flow (IBF) remain largely unexplored.

Daikenchuto (TU-100), a traditional Japanese herbal medicine (Kampo), is a mixture of extract powders from dried Japanese pepper, processed ginger, ginseng radix, and maltose powder. TU-100 is the most frequently prescribed Kampo medicine in Japan, especially for the treatment of postoperative paralytic and adhesive ileus and ischemic intestinal disorders (28). Basic studies have demonstrated the effect of TU-100 on intestinal motility, adhesion, vasodilatation, inflammation, and bacterial translocation (15, 22, 25, 27, 29, 30, 38, 44–47, 51, 52, 58). In a previous study, we demonstrated that TU-100 increases IBF via enhancement of adrenomedullin (ADM) release from the intestinal epithelial (IE) cells (27). However, the mechanism by which TU-100 enhances ADM release has not been elucidated.

Because some of the major ingredients of TU-100, such as 6-shogaol (6SG) and hydroxy-α-sanshool (HAS), are regarded as TRP vanilloid type 1 (TRPV1)/TRP ankyrin 1 (TRPA1) agonists (21, 31), we hypothesized that TRPV1/TRPA1 stimulation increases IBF via enhancement of ADM release from IE cells, and that the beneficial effect of TU-100 on IBF is mediated by this mechanism. Our results strongly suggest that TRPA1 present in IE cells controls IBF via ADM release and, therefore, the stimulation of intraluminal TRPA1 may be a promising approach for the relief of abdominal symptoms in various intestinal disorders associated with impaired IBF.

MATERIALS AND METHODS

Test sample and reagents. TU-100 is an aqueous extract containing processed ginger, ginseng radix, and Japanese pepper in a ratio of 5:3:2. The dried powdered extract form of TU-100 was obtained from Tsumura and Co. (Tokyo, Japan). The yield of the extract was 12.5%. TU-100 is prepared by mixing TU-100 extract powder and maltose syrup powder (Tsumura and Co.) at a ratio of 1:8. Although the doses of TU-100 in the present study (270–2,700 mg/kg body wt) are higher than the clinical doses used in humans, previous studies in animals have shown that the relevant pharmacological effects occur only in the experimental doses. Furthermore, treatment of rodents with TU-100 at this higher dose range results in blood concentrations of major TU-100 constituents that are similar to those detected in human volunteers treated with TU-100 at clinical dose range (18, 37).

Ginsenoside Rb1, ginsenoside Rg1, ginsenoside Rd, protopanaxadiol, 6SG, 6-gingerol, 10-gingerol, maltose, allyl-isothiocyanate (AITC), and capsaicin (CAP) were purchased from Wako Pure Chemical Industries (Osaka, Japan). Urethane, α-chloralose, cinnamalde-

Address for reprint requests and other correspondence: T. Kono, Center for Clinical and Biomedical Research, Sapporo Hisgashi Tokushukai Hospital, 14-3-1 Higashi, N33, Higashi-ku, Sapporo, Hokkaido 065-0033, Japan (e-mail: kono@asahikawa-med.ac.jp).

hyde (CNA), methyl cinnamate, 2-aminoethoxydiphenyl borate (2-APB), 4α-phorbol 12,13-didecanoate (4α-PDD), H-89, calphostatin C, LY294002, and phorbol 12-myristate 13-acetate (PMA) were purchased from Sigma Aldrich (St. Louis, MO). HAS and hydroxy-β-sanshool (HBS) were extracted from Japanese pepper at Tsumura and Co. with purities greater than 97.9%. Xanthoxylin (Tokyo Chemical Industry, Tokyo), butorphanol (Bristol-Myers Squibb, New York), HC-030031 (Biomol International, Plymouth Meeting, PA), and *N*-(4-tertiarybutylphenyl)-4-(3-chloropyridin-2-yl)-tetrahydropyrazine-1(2H) carboxamide (BCTC; Biomol International) purchased for the study as well the other reagents used for analysis were the highest purity commercially available.

Animals. Seven-week-old male Sprague-Dawley rats weighing 210–230 g were purchased from Japan SLC (Shizuoka, Japan). The animals were allowed free access to water and standard laboratory food, and housed at a temperature of 23 ± 2°C with relative humidity of 55 ± 10%, and a 12:12-h light/dark cycle with lights on from 0700–1900 daily. All experimental procedures were performed according to the Guidelines for the Care and Use of Laboratory Animals of Asahikawa Medical University or Tsumura and Co. Ethical approval for the experimental procedures used in this study was obtained from the Laboratory Animal Committee of Asahikawa Medical University or Tsumura and Co. All animal procedures were in accordance with the National Institutes of Health Guide for the Care and Use of Laboratory Animals.

Measurement of intestinal blood flow. Jejunal blood flow was measured by a laser-Doppler flowmeter (ALF21N, Advance, Tokyo) as previously described (30). Briefly, rats were anesthetized with urethane (900 mg/kg ip), α-chloralose (45 mg/kg ip), and butorphanol (1 mg/kg im). A tracheotomy was performed and the rats were artificially ventilated. The left cervical artery was cannulated and connected to a transducer (P23XL, Nihon Kohden, Tokyo) to monitor systemic arterial blood pressure (AP) and heart rate (HR). Body temperature was maintained at 37 ± 0.5°C by a heating pad. After exposing the small intestine by a midline laparotomy, a cannula was inserted into the duodenum to facilitate injection of the test sample. A fiber optic probe was positioned 4 mm above the surface of the midjejunum. Vascular conductance (VC), calculated as the quotient of mean blood flow divided by mean AP, was used as an index of IBF.

Antagonist and antibody studies in vivo. Rabbit polyclonal IgG (50 μg/kg) against rat ADM (Peninsula Laboratory, Belmont, CA), rabbit IgG as an isotype-matched control (Abcam, Cambridge, UK), or the TRPV1 antagonist BCTC (10 mg/kg) was injected at a volume of 1 ml/kg through a polyethylene tube cannulated into the right jugular vein after confirming stable blood flow. TU-100 or a related vasodilator was administered intraduodenally 15 min later. The TRPA1 antagonist HC-030031 prepared in 1% DMSO was administered into the lumen at 1 mg·5 ml $^{-1}$·kg $^{-1}$ together with the test sample.

Quantitation of ADM. Plasma ADM levels were assayed using enzyme immunoassay (EIA) kits specific for rat ADM according to the procedure provided by the manufacturer (Phoenix Pharmaceuticals, Burlingame, CA). Briefly, 5 ml blood was collected from the portal vein at 15, 30, 60, and 120 min after administration of TU-100 (2,700 mg/kg), and plasma was separated immediately. The plasma was then applied to ADM extraction using a C18 Sep-Column. The detection limit for ADM was 10 pg/ml. ADM release was assayed using an IEC-6 rat intestinal epithelial cell line (DS Pharmaceuticals, Osaka, Japan). IEC-6 cells were grown in DMEM supplemented with 10% heat-inactivated FBS, 2 mmol/l L-glutamine, 100 U/ml penicillin, 100 μg/ml streptomycin, and 10 mmol/l HEPES. Cells between the 30th and 37th passage were plated in 96-well flat-bottom microtiter plates at 2 × 10^4 cells/well in DMEM supplemented with the same additives as described above, allowed to settle overnight, and then culture fluids were replaced with HBSS containing 0.1% BSA, 0.1–0.3% DMSO. TU-100 was added to the culture after being passed through a 0.45-μm filter. Cells were incubated for 6 h, and ADM in the culture fluids was quantified using EIA kits specific for rat ADM. To investigate functional expression of TRPA1 in IEC-6 cells, the cell was exposed to the TRPA1-selective antagonist HC-030031 (100 μmol/l) 30 min before addition of TRPA1 activators.

Preparation of IE cells from small intestine. Segments of the small intestine were everted, end-ligated, and preincubated in HBSS containing 1 mmol/l DTT and 10% FBS to remove mucus. The sacs were then incubated for 10 min at 37°C in chelating digestive buffer (70 mmol/l NaCl, 5 mmol/l KCl, 20 mmol/l $NaHCO_3$, 0.5 mmol/l NaH_2PO_4, 1 mmol/l Na_2HPO_4, 50 mmol/l HEPES, 11 mmol/l glucose, 1 mmol/l EDTA, 0.5% BSA, and 0.05 mmol/l DTT), followed by collection of the supernatant. The incubation was repeated twice, and the supernatants of each were pooled. The cell pellets obtained by centrifugation at 300 *g* for 10 min were suspended in 0.1% BSA HBSS and passed through a nylon mesh filter. The cell suspension was applied to a 25% gradient of Percoll (GE Healthcare, Piscataway, NJ). After centrifugation at 710 *g* for 30 min, the interface containing enriched IE cells was collected. IE cells were separated into negative fractions using a BD IMag cell separation system (BD Biosciences, San Jose, CA) with rabbit anti-nerve growth factor receptor p75 antibody (Millipore, Bedford, MA), followed by biotinylated anti-rabbit Ig (BD Bioscience) and biotinylated anti-CD45 antibody (clone, OX-1; BD Bioscience), and thereafter incubated with streptavidin-labeled magnetic beads. Further, purified IE cells were stained with various cell-marker antibodies following a cytospin. Antibodies and positive cell percentages were wide cross-reactivity anti-cytokeratin (DAKO, Carpinteria, CA) at ≥90%, and anti-E-cadherin (clone, 36/E-cadherin; BD Bioscience) at ≥95%. Positive staining with anti-CD45 (clone, OX-1; BD Bioscience), anti-PGP9.5 (clone, 13C4/I3C4; Abcam), or anti-GFAP (clone, GF12.24; Progen, Heidelberg, Germany) was not detected.

Gene expression. The pellets of IEC-6 cells, enriched IE cells obtained from the small intestines, and L1 to L6 dorsal root ganglia (DRG) isolated from normal rats were homogenized in QIAzol reagent (Qiagen, Valencia, CA), and total RNA was isolated using an RNeasy kit (Qiagen) according to the manufacturer's recommendations. The respective cDNA was prepared using a high-capacity RT kit (Applied Biosystems, Warrington, UK). The sequences of the sense and antisense primers for rat TRPA1 were 5′-TTTGCCGCCAGCTATGGGCG-3′ and 5′-TGCTGCCAGATGGAGAGGGGT-3′ to obtain a 117-bp product. Those for rat TRPV1 were 5′-GGTGTGCCTGCACCTAGC-3′ and 5′-CTCTTGGGGTGGGGACTC-3′ to obtain a 107-bp product. Those for rat ADM were 5′-CTCGACACTTCCTCGCAGTT-3′ and 5′-GCTGGAGCTGAGTGTGTCTG-3′ to obtain a 446-bp product. Those for rat β-actin were 5′-CCTGGGTATGGAATCCTGTGGCAT-3′ and 5′-GGAGCAATGATCTTGATCTTC-3′ to obtain a 198-bp product. An aliquot of the RT reaction product served as a template in 30 cycles with 10 s of denaturation at 98°C, 30 s of annealing at 60°C, and 30 s of extension at 68°C using the DNA polymerase KOD FX (TOYOBO, Osaka, Japan). A portion of the PCR mixture was electrophoresed on 2% agarose gel in Tris-acetate-EDTA buffer (pH 8.0), and the gel was stained with ethidium bromide and imaged on a Typhoon 9410 imager (GE Healthcare). Sample-to-sample variation in RNA loading was controlled by comparison with β-actin.

Flow cytometry. Single cells were suspended in Cytofix/Cytoperm solution (BD Biosciences) for 20 min at 4°C, washed, and then preincubated for 5 min at 4°C with goat polyclonal IgG antibody (Abcam) to reduce nonspecific binding of antibodies. Next, cells were incubated for 20 min at 4°C with rabbit polyclonal IgG antibody (4 μg/ml) against rat ADM, rat TRPA1 (Abcam), TRPV1 (Alomone Labs, Jerusalem, Israel), or isotype control IgG (Abcam). Cells were washed, incubated for 20 min with the Alexa Fluor 488-labeled goat polyclonal antibody against rabbit IgG (Invitrogen, Carlsbad, CA), and subjected to flow cytometry analysis using a FACScalibur analyzer and CellQuest Pro software (BD Biosciences). In some experiments, a control peptide for TRPA1 or TRPV1 (Abcam) was added at 4 μg/ml with antigen-specific antibody.